Catalysis Today 343 (2020) 56–62

Contents lists available at ScienceDirect

Catalysis Today

journal homepage: www.elsevier.com/locate/cattod

Stable niobia-supported nickel catalysts for the hydrogenation of carbon monoxide to hydrocarbons

C. Hernández Mejía, C. Vogt, B.M. Weckhuysen, K.P. de Jong*

Inorganic Chemistry and Catalysis, Debye Institute for Nanomaterial Science, Utrecht University, Universiteitsweg 99, 3584 CG Utrecht, P.O. Box 80083, 3508 TB, Utrecht, the Netherlands

ARTICLE INFO

Keywords:
Nickel catalysts
Sintering
Strong metal-support interaction
Hydrocarbon synthesis
Metal nanoparticles

ABSTRACT

Stability of metal nanoparticles under reaction conditions is crucial in many catalytic processes. Nickel-based catalysts often encounter severe particle growth in the presence of carbon monoxide due to the formation and migration of nickel carbonyl. In this research, we showed that the reduction temperature of nickel oxide supported on niobia (Nb_2O_5) influenced the stability of the resulting nickel catalyst during subsequent carbon monoxide hydrogenation. Low reduction temperatures resulted in high initial nickel-normalized activity towards long-chain hydrocarbons (C_{5+}), but fast deactivation throughout the experiment. High reduction temperatures led to a shift in product distribution towards shorter hydrocarbons and a decreased initial nickel-normalized activity, while during the first hours of the experiment an increase in turnover frequency and nickel-normalized activity was observed, resulting eventually in a stable catalytic performance. Electron microscopy analysis revealed extensive particle growth after catalysis when the catalyst had been reduced at low temperatures and no significant changes in particle size when reduced at high temperatures. By use of *in-situ* FT-IR spectroscopy, nickel subcarbonyl species which are precursors of volatile nickel tetracarbonyl were detected on Ni/Nb_2O_5 after low temperature reduction and exposure to CO, but not after high temperature reduction. Hence, particle growth is explained by the formation and diffusion of nickel carbonyl and subsequent Ostwald ripening, that leads to larger nickel particles with concomitant decrease in nickel-normalized activity. The stability of the catalyst reduced at high temperature was linked to the formation of niobium suboxides and their partial coverage of the nickel particles limiting the formation of nickel carbonyl and slowing down particle growth.

1. Introduction

Metal nanoparticles are commonly used to catalyze many chemical processes [1]. Since catalytic reactions occur at the metal surface, the high surface-area-to-volume-ratio of a nanoparticle provides an effective number of active sites per weight of metal in the overall catalyst. One of the biggest challenges for any catalytic system is to maintain this maximum amount of active sites throughout the lifespan of a solid catalyst [2]. Particularly in the case of metal nanoparticles, their growth is a prevailing phenomenon in which the efficient utilization of the metal in a catalyst is compromised, usually leading to a detriment in catalytic performance [3–5]. In order to stabilize the nanoparticles and prevent their growth, these are typically dispersed over a support material. The nature of the support is crucial in delivering this stability and offers an opportunity to develop improved solid catalysts.

Reducible oxides used as support material display characteristic interactions with metal nanoparticles. During reductive conditions, one effect that arises is coverage of the nanoparticles by *in-situ* generated suboxides from the support [6,7], the so called Strong Metal-Support Interaction (SMSI) [8,9]. This effect can modify the available metal surface area, the electronic state of the metal and the particle shape [10–12]. An interesting example is the substantial change in reactivity of nickel during carbon monoxide hydrogenation: nickel supported on non-reducible oxides (e.g. Al_2O_3, SiO_2) selectively hydrogenates carbon monoxide to methane, whereas when supported on reducible oxides like TiO_2 or Nb_2O_5 the product distribution shifts towards heavier hydrocarbons [13–17]. Furthermore, previous reports have suggested that reducible supports can also deliver unique stability to nickel-based catalysts [13,18].

The interest to achieve stable nickel-based systems in the presence of carbon monoxide arises from the extensive utilization of nickel catalysts in reactions involving carbon monoxide as reactant, intermediate or product [19–23] and the poor stability of nickel in the presence of carbon monoxide at low temperatures [24,25]. Deactivation of nickel-

* Corresponding author.
E-mail address: k.p.dejong@uu.nl (K.P. de Jong).

https://doi.org/10.1016/j.cattod.2018.11.036
Received 17 August 2018; Received in revised form 12 November 2018; Accepted 15 November 2018
Available online 22 November 2018

based catalysts during carbon monoxide hydrogenation proceeds most often through particle growth by the formation and diffusion of volatile nickel carbonyl [25–27]. This phenomenon is a classic example of Ostwald ripening, where species containing metal atoms, in this case nickel carbonyl, diffuse from smaller towards larger nanoparticles leading to metal sintering [28,29]. In order to prevent this, the reaction is typically operated at high temperatures and low CO pressures, since these conditions disfavor the formation of nickel carbonyl [24,26,30]. However, such conditions compromise the product selectivity mainly towards methane and therefore hamper the application of nickel catalysts for the synthesis of more commercially attractive products, such as long-chain hydrocarbons (C_{5+}) or olefins [31,32]. Alternative strategies to inhibit the formation of nickel carbonyl in these catalysts have been explored in literature, for instance, by alloying nickel with copper [33,34] or by depositing nickel on titania, a reducible support [13].

Here, we studied the effect of SMSI in nickel supported on niobia for the hydrogenation of carbon monoxide. For this, different reduction temperatures (250–450 °C) on NiO/Nb_2O_5 were used prior to H_2-chemisorption, in order to determine the extent of SMSI, and prior to CO hydrogenation. H_2-uptake suppression was observed when increasing the reduction temperature which is characteristic of the SMSI effect. Simultaneously, an increase in reduction temperature led to a decrease in nickel-based catalytic activity, however stable catalytic performance was gained in return with high selectivity for long-chain hydrocarbons. Ni/Nb_2O_5 showed higher turnover frequency and C_{5+} selectivity compared to nickel supported on a non-reducible support (α-Al_2O_3). The overall results obtained pointed out to an inhibition of nickel carbonyl formation by SMSI in Ni/Nb_2O_5, leading to a stable supported nickel catalyst for CO hydrogenation.

2. Experimental

2.1. Catalysts preparation

Niobium oxide (Nb_2O_5) was used as support and obtained by crystallization of niobium oxide hydrate (Nb_2O_5•nH_2O, HY-340, AD/4465), which was provided by Companhia Brasileira de Metalurgia e Mineração – CBMM. The crystallization was carried out in stagnant air at 600 °C during 4 h with a ramp of 5 °C min^{-1}. The obtained Nb_2O_5 had a pseudo-hexagonal TT-phase, a specific surface area of 9 m^2 g^{-1} and a specific mesopore volume of 0.05 cm^3 g^{-1}.

A nickel supported on niobia catalyst was prepared using the incipient wetness impregnation method. Prior to impregnation the support (75–150 µm grains) was dried under vacuum at 80 °C for 1 h, thereafter the impregnation was performed at room temperature with a 4.2 M aqueous solution of $Ni(NO_3)_2$•$6H_2O$ (Acros, 99%) for a 6 wt.% Ni. In the next step, the catalyst was dried for 1 h at 60 °C in a fixed bed reactor under N_2 flow and subsequently in the same reactor and gas flow calcined for 2 h at 350 °C (3 °C min^{-1}). Nickel supported on α-alumina (BASF) was prepared in the same way. Metal loadings were defined as the mass of metallic Ni per gram of reduced catalyst.

2.2. Characterization

Temperature programmed reduction (TPR) analyses were performed using a Micromeritics Autochem 2990 instrument, where 100 mg sample was dried at 120 °C for 1 h in Ar flow followed by reduction from room temperature up to 700 or 1000 °C (5 °C min^{-1}) in a 5 vol% H_2/Ar flow. Powder X-ray diffractograms were measured using a Bruker-AXS D2 Phaser X-ray diffractometer, Co-Kα radiation (λ = 1.789 Å). Bright field transmission electron microscopy (TEM) and Scanning transmission electron microscopy (STEM-EDX) images were acquired with a Philips Tecnai-20 FEG (200 kV) microscope equipped with an energy dispersive X-ray (EDX) and high-angle annular dark-field (HAADF) detector. The reduced and subsequently passivated samples for the microscopy analysis were prepared by suspending the catalysts in 2-propanol (> 99.9%, Sigma-Aldrich) using sonication and dropcasting the suspension on a carbon-coated Cu grid (200 mesh). The nickel particle size was determined using the iTEM software by analyzing at least 500 particles. Particle surface average diameters or Sauter mean (D[3,2]) were then calculated and corrected for a 2 nm NiO shell [35]. H_2-chemisorption was measured on a Micromeritics ASAP 2020C using ~100 mg of sample. Prior to the measurement, the calcined catalyst was reduced in H_2 flow at different temperatures during 2 h (5 °C min^{-1}). The sample was then evacuated, cooled to 150 °C and H_2-chemisorption was measured at that temperature. Inductively coupled plasma-optical emission spectroscopy (ICP-OES) was performed on a SPECTRO ARCOS in order to establish the nickel content before and after catalysis; samples were extracted using aqua regia.

Fourier-transform Infrared (FT-IR) spectroscopy measurements were carried out in a Specac "High Temperature High Pressure" transmission FT-IR cell. A self-supported catalyst wafer was prepared by applying on a sample a force of 4000 kg for 20 s, yielding a wafer of 16 mm diameter, and < 1 mm thickness. Catalyst wafers were reduced *in-situ*, each at different temperatures of 250, 350 and 450 °C (N_2/H_2 = 2 v/v; both Linde, 5.0). Subsequently, a sample was cooled down to 230 °C flushed with 5.0 purity N_2 for 10 min, after which flowing CO (Linde, 5.0) was added with a ratio N_2/CO = 2 v/v at 1 bar total pressure. Due to low photon-transmittance of the Nb_2O_5-supported Ni catalyst, 256 spectra were averaged to improve signal-to-noise. Spectra were recorded with a resolution of 4 cm^{-1}.

2.3. Catalytic performance

Catalytic performance was carried out in a quartz glass plug-flow reactor, loaded with 15–20 mg catalyst (38–150 µm) diluted with ~200 mg SiC. Catalysts were reduced in situ at 250, 350 or 450 °C (5 °C min^{-1}, 2 h) in an Ar/H_2 = 2.0 v/v flow (GHSV = 190 000 h^{-1}). After reduction, CO hydrogenation was performed at 230 °C, 1 bar, H_2/CO = 2.0 v/v, GHSV = 28 000 h^{-1} and CO conversion < 5%. Reaction was carried out for 90 h. Finally, the CO flow was stopped and the H_2 flow and temperature were kept for one hour in order to remove remaining hydrocarbons for further analysis of the catalyst. C_1-C_{18} products were analyzed by online gas chromatography (Varian 430 GC, CP sil-5 column).

3. Results and discussion

A nickel supported on niobia catalyst was synthetized by incipient wetness impregnation method. After subsequent drying and calcination, the nickel content was determined by ICP-OES, being 5.6 ± 0.1 wt.%. Nickel supported on α-alumina was also synthetized as comparative system, with a nickel content of 5.5 ± 0.1 wt.% as determined by ICP-OES. Temperature programed reduction was carried out on the support (Nb_2O_5), the calcined NiO/Nb_2O_5 and NiO/α-Al_2O_3 samples. The corresponding reduction profiles for the niobia-based samples are shown in Fig. 1. Nb_2O_5 showed a gradual consumption of hydrogen starting at 600 °C and a maximum consumption rate at 940 °C. The hydrogen consumption was assigned to the reduction of the Nb_2O_5 surface to NbO_2, along with the change in color of the sample to deep indigo, characteristic of Nb^{4+} ions [36,37]. The reduction profile for the NiO/Nb_2O_5 sample showed a small hydrogen consumption signal at 200 °C which might be attributed to the reduction of Ni^{3+}. The main hydrogen consumption between 230 and 430 °C was attributed to the reduction of NiO to metallic Ni [38,39]. Hydrogen consumption continued above 700 °C related to reduction of Nb_2O_5, catalyzed by the metallic nickel [40]. The consumption peak at 780 °C might correspond to the initial reduction of the support surface (Nb_2O_5 to NbO_2) and further consumption above 810 °C to the reduction of bulk Nb_2O_5 and possibly subsequent reduction of NbO_2 to Nb_2O_3. Nickel oxide supported on α-Al_2O_3 showed a similar reduction profile to the niobia-based sample (Figure S1), with a small hydrogen consumption signal at

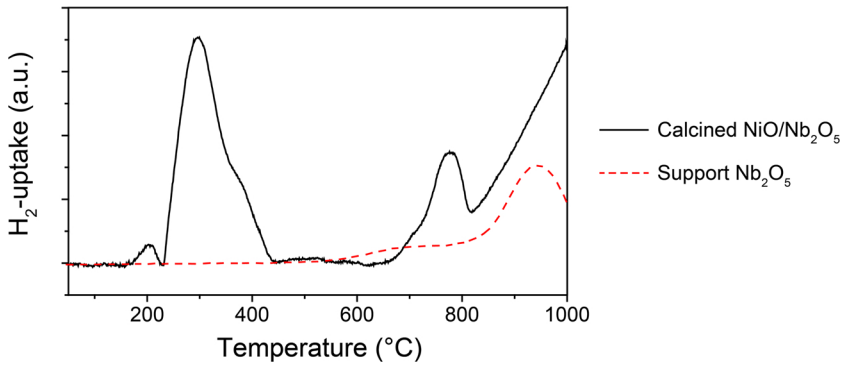

Fig. 1. H_2–TPR profile of the Nb_2O_5 support (red dashed line) and of the calcined NiO/Nb_2O_5 sample (black line) (For interpretation of the references to colour in this figure legend, the reader is referred to the web version of this article).

220 °C ascribed to Ni^{3+} reduction and a main signal between 250 and 450 °C for NiO reduction to Ni. For both Nb_2O_5- and α-Al_2O_3-supported samples, the total hydrogen consumption below 450 °C corresponded to the complete reduction of all nickel oxide to metallic nickel.

Based on the NiO/Nb_2O_5 TPR profile, four different reduction temperatures, namely 250, 350 and 450 °C, were chosen to study their effect on CO hydrogenation. The degree of reduction for the low temperatures (250 and 350 °C) was calculated by measuring TPR of NiO/Nb_2O_5 with an additional dwell step of 2 h at 250 or at 350 °C. The isothermal step at 250 °C resulted in two main distinctive signals in hydrogen uptake for the reduction of nickel oxide (Figure S2, A). The first one was observed by reaching 250 °C with a sharp increase in hydrogen uptake which gradually decreased back to the baseline throughout the 2 h at 250 °C. Based on the hydrogen uptake the degree of reduction at this temperature was 58%. The second main hydrogen uptake signal was observed after the isothermal step with a maximum at 360 °C (t = 200 min), this indicates that temperatures higher than 250 °C are necessary to completely reduce the nickel oxide to metallic nickel. The hydrogen uptake observed at 360 °C might relate to the observed shoulder at the same temperature in Fig. 1, which might correspond to the reduction of nickel oxide species with a stronger interaction with the support. The TPR profile with an isotherm step at 350 °C (Figure S2, B) showed a main hydrogen uptake signal which corresponded to a degree of reduction of 96%, indicating that most of the nickel oxide is reduced to metallic nickel at 350 °C.

Table 1 shows the hydrogen uptake determined by H_2-chemisorption for Ni/Nb_2O_5 and Ni/α-Al_2O_3 after reduction at different temperatures. An increase of the reduction temperature resulted in a decrease in hydrogen uptake for Ni/Nb_2O_5, resulting in an apparent increase in the derived particle size. This suppression of hydrogen chemisorption by reducible oxidic supports, the so called strong metal-support interaction (SMSI) effect, is a well-documented phenomenon attributed to coverage of the metal nanoparticles by suboxides from the support upon reductive conditions [6,8]. The degree of coverage by the suboxides is a temperature-dependent phenomenon, in which higher reduction temperatures enhance the mobility of these species and coverage of the nanoparticles [41]. Powder X-ray diffraction (Figure S3) neither showed the formation of new crystalline species (e.g. nickel niobates) nor provided indications of SMSI after reduction of Ni/Nb_2O_5. Reduction at 250 °C showed a substantial hydrogen uptake even though nickel oxide was not completely reduced at 250 °C as shown by the TPR results, indicating that most of the particles' surface consisted of metallic nickel. The Ni/α-Al_2O_3 sample showed also a decreased in the hydrogen uptake upon increasing the reduction temperature, however this decrease was not as severe as the one observed for Ni/Nb_2O_5. After the chemisorption measurement and exposure to air at room temperature, the samples were analyzed by TEM (Fig. 2 and Figure S4). TEM images showed for all Ni/Nb_2O_5 samples a uniform distribution of nickel nanoparticles over the niobia. Furthermore, a similar nickel particle size (~ 12 nm) was determined based on TEM as shown in Table 1, indicating no significant effect of the reduction temperature on the nickel particle size and confirming that the suppressed hydrogen chemisorption results related to the SMSI effect. In the case of the Ni/α-Al_2O_3 sample, TEM images (Figure S4) revealed a slight increase in particle size upon increasing the reduction temperature, in line with the results obtained from hydrogen chemisorption. The discrepancy observed here between the experimental and theoretical H_2-uptake can be explained by the more significant impact of larger particles when determining the D[3,2] value, a surface-based diameter. Since a considerable amount of very small nanoparticles would not be detected by TEM.

Table 1
H_2-uptake for Ni/Nb_2O_5 at different reduction temperatures measured by chemisorption.

		H_2-chemisorption		TEM	
Support	Reduction Temperature (°C)	Experimental H_2-uptake ($\mu mol \cdot g_{Ni}^{-1}$)	Particle size (nm)	Particle size D [3,2] (nm)	Theoretical H_2-uptake ($\mu mol \cdot g_{Ni}^{-1}$)
Nb_2O_5	250	936	10	12	716
	350	626	15	12	740
	450	16	539	11	785
α-Al_2O_3	350	1328	6	9	955
	450	1078	8	12	716

The catalytic performance of the Ni/Nb_2O_5 and Ni/α-Al_2O_3 catalysts was evaluated by varying the reduction temperatures similar to the H_2-chemisorption experiments. The results are shown in Fig. 3 where nickel-normalized catalytic activity (Nickel Time Yield, NTY) is plotted against time-on-stream (TOS) up to 90 h, furthermore a summary of the catalytic performance is shown in Table 2. The initial NTY (TOS = 0) showed consistency with the H_2-chemisorption results, i.e. reduction at low temperatures for the niobia-supported sample displayed high H_2-uptake along with markedly high initial NTY whereas an increase of the reduction temperature led to a suppression of the H_2-uptake and a decrease in the initial NTY. However, the decrease in initial NTY is not proportional to the decrease in H_2-uptake for unknown reasons. The stability throughout time significantly varied for each reduction temperature. Reduction at 250 °C led to severe deactivation, down to 70% loss in NTY at TOS = 90 h. A less pronounced deactivation was observed when the reduction temperature was increased to 350 °C with only 40% loss in NTY, however the catalyst did not reach steady state during the experiment due to continuous deactivation. In stark contrast, reduction at 450 °C showed a catalytic performance, with a low initial NTY which increased during the first 30 h of the reaction followed by a stable conversion until the end of the experiment. This might indicate a partial recover of the available

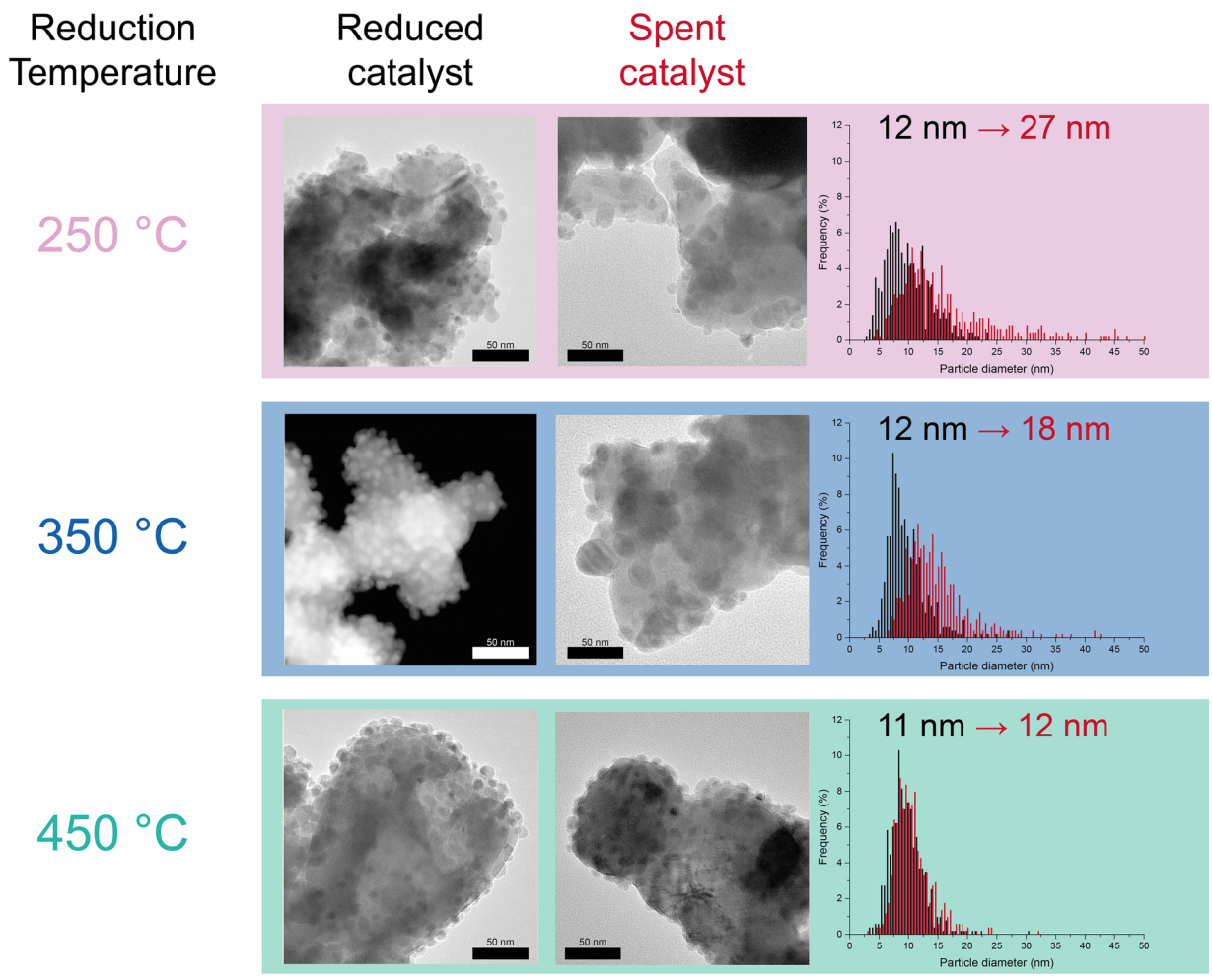

Fig. 2. TEM images of the Ni/Nb_2O_5 catalyst after reduction at different temperatures and passivation (denoted as reduced) and after catalysis (denoted as spent). The corresponding histograms show the particle size distribution for the 'reduced' (black bars) and 'spent' (red bars) with their corresponding surface-average particle sizes. (For interpretation of the references to colour in this figure legend, the reader is referred to the web version of this article).

metallic surface area during reaction conditions, which has been associated in literature to re-oxidation of the suboxides (e.g. NbO_x) by water produced during reaction, hence modifying the SMSI effect [42]. Contrary to the Ni/Nb_2O_5 sample, the reduction temperature had a minor effect on the catalytic performance of the $Ni/\alpha\text{-}Al_2O_3$ as shown in Fig. 3. Reduction at 350 °C led to a small increase in NTY than when reduced at 450 °C at the beginning of the experiment, this difference originated from their different initial particle size as revealed by their same initial turnover frequencies (TOF). Their prevalent decrease in NTY during the experiment resulted in almost similar NTY values at

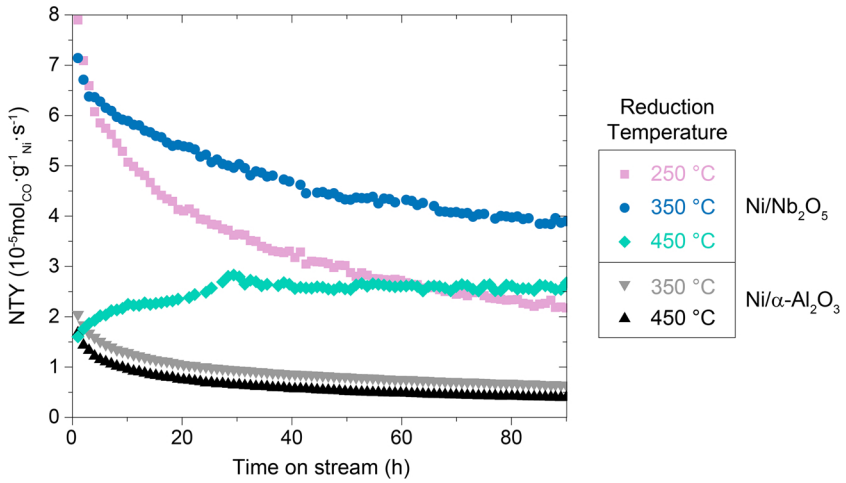

Fig. 3. Nickel Time Yield (NTY) plotted against time-on-stream for Ni/Nb_2O_5 and $Ni/\alpha\text{-}Al_2O_3$ reduced at different temperatures prior to reaction. *In-situ* reduction: 1 bar, Ar/H_2 = 2 v/v, GHSV = 190 000 h^{-1}, T = 250–450 °C. Reaction conditions: 1 bar, H_2/CO = 2 v/v, GHSV = 28 000 h^{-1}, T = 230 °C, CO conversion: 1–4 %.

Table 2
Summary of the catalytic performance for the Ni/Nb_2O_5 and $Ni/\alpha\text{-}Al_2O_3$ catalysts. Reaction conditions: 230 °C, 1 bar, H_2/CO = 2.0 v/v, GHSV = 28 000 h^{-1} and CO conversion < 5%.

Support	Reduction Temperature (°C)	NTY (10^{-5} molCO·g_{Ni}^{-1}·s^{-1})		TOF[a] (10^{-3} s^{-1})		TOF_{app}[b] (10^{-3} s^{-1})	Selectivity[c] (wt.%)			α[d]	Olefin/Paraffin[e]
		TOS = 0 h	TOS = 90 h	TOS = 0 h	TOS = 90 h	TOS = 0 h	C_1	C_2-C_4	C_{5+}		
Nb_2O_5	250	7.9	2.2	46	39	42	18	33	49	0.65	0.9
	350	7.1	3.9	45	42	59	15	30	55	0.70	1.0
	450	1.6	2.7	11	20	605	22	45	33	0.58	1.6
$\alpha\text{-}Al_2O_3$	350	2.0	0.6	11	10	8	54	35	11	0.46	0.8
	450	1.7	0.5	12	8	8	55	35	10	0.45	0.9

[a] Based on TEM particle size distribution in fresh (for TOS = 0 h) and spent (for TOS = 90 h) catalyst.
[b] Based on H_2-chemisorption of fresh catalyst.
[c] Selectivity is reported at TOS = 90 h and up to C_{18}.
[d] Values were determined for C_1-C_{11} concentration values.
[e] Molar ratios determined for C_4-C_7.

TOS = 90 h. The niobia-supported sample showed independently of the reduction temperature higher NTY values than the alumina-supported sample at the end of the experiment. The nickel content was determined after catalysis by ICP-OES showing no metal loss during the experiment for all samples.

The promotional effect of niobia was maintained in all cases as shown by the TOFs compared to $Ni/\alpha\text{-}Al_2O_3$, determined either by particle size distribution from TEM or H_2-chemisorption (Table 2). Initial TOFs based on TEM particle size distributions showed the highest values for Ni/Nb_2O_5 reduced at low temperatures (250 and 350 °C) and decreased when increasing the reduction temperature to 450 °C. The inverse trend was observed for the apparent initial TOFs based on chemisorption results (TOF_{app}, Table 2); an increase in reduction temperature led to a substantial increase in TOF_{app} due to the hydrogen chemisorption suppression by SMSI (vide supra). However, the nickel surface under reaction conditions is expected to change and therefore these TOFs are indicated as 'apparent'. Interestingly, Ni/Nb_2O_5 reduced at 250 °C shows consistent values for both initial TOFs indicating that coverage of the nickel nanoparticles by suboxides from the support has not taken place at this temperature. Consequently, the resulting high TOF might originate from the interphase of the nickel nanoparticles and the support. For $Ni/\alpha\text{-}Al_2O_3$, the apparent TOFs and TOFs based on TEM have the same values and SMSI does not play a role in this catalyst system.

The change in reduction temperature additionally influenced the selectivity of the nioba-supported catalyst, as shown with the Anderson–Schulz–Flory (ASF) product distribution plot in Fig. 4 and in Table 2. For all reduction temperatures, niobia-supported catalysts showed higher selectivity towards long-chain hydrocarbons when compared to the alumina-supported catalyst. At TOS = 90 h, the catalyst reduced at 350 °C had the highest α value, with the highest selectivity to C_{5+} products, followed by the reduction temperature at 250 °C. Reduction at 450 °C led to a shift in product distribution to shorter hydrocarbons and therefore a smaller α value. Suppressed C_2H_4/C_2H_6 was observed for the catalyst reduced at 250 or 350 °C, which has been attributed in the case of cobalt-based catalysts to re-adsorption of olefins to the metal surface to further increase chain-growth [43,44]. However, reduction at 450 °C did not show this behavior, instead a slight increase in the olefin selectivity was observed, as shown in Table 2. Re-adsorption of olefins could be hindered on the metal surface, shifting the selectivity to shorter hydrocarbons. On the other hand, $Ni/\alpha\text{-}Al_2O_3$ showed the lowest α value, a high selectivity for methane and to a lesser extent for C_2 to C_{10} products for both reduction temperatures. The formation of C_{2+} products in this case might be due to some small nickel metal nanoparticles (< 3 nm) found in this catalyst (Figure S4), which agrees with previous research reports [45].

The Ni/Nb_2O_5 samples after catalysis were analyzed by TEM and the results are shown in Fig. 2. Significant changes for the nickel

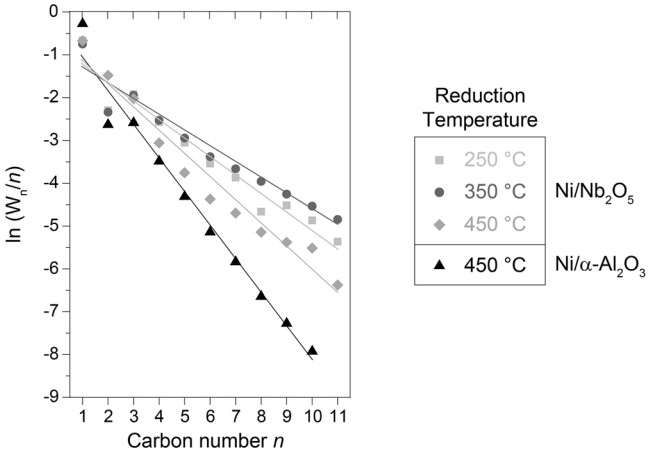

Fig. 4. Anderson–Schulz–Flory-plot (ASF-plot) at TOS = 90 h for Ni/Nb_2O_5 after different reduction temperatures and for the $Ni/\alpha\text{-}Al_2O_3$ reference catalyst. W_n = weight fraction of olefins plus paraffins of given carbon number n in total hydrocarbon products.

nanoparticles were observed for the spent catalyst reduced at 250 °C: broadened particle size distribution and increased average particle size (12 nm to 27 nm) were observed. Likewise, large particles were observed for the spent catalyst after reduction at 350 °C leading to a particle mean size of 18 nm. The observed nickel particle growth agreed with the stability of the catalyst during reaction; where reduction at 250 °C led to the severest deactivation and the most pronounced particle growth, increase of the reduction temperature to 350 °C attenuated the particle growth and diminished the deactivation rate. The resulting particle sizes and catalytic activity at TOS = 90 h led to similar TOFs for both reduction temperatures when compared to initial TOFs (Table 2). This is an indication that the decrease in NTY was mainly due to particle growth. The slight decrease in TOF might relate to carbon deposition over the nickel surface. In a similar way, TEM of the spent $Ni/\alpha\text{-}Al_2O_3$ catalysts revealed a substantial increase in nickel particle size (Figure S5), indicating that the decrease in NTY originated mainly from particle growth. Particle growth for nickel-based catalysts under these reaction conditions most likely occurs via Ostwald ripening by the formation of $Ni(CO)_4$ [25–27]. In contrast, the nickel particles remained well distributed over the support for the Ni/Nb_2O_5 sample reduced at 450 °C. No significant change in particle size was observed after catalysis, with a final mean particle size of 12 nm. Therefore, the increase in CO conversion during the first hours of the experiment means that sites more active became available and thus the TOF almost doubled (Table 2). These results suggest that SMSI inhibited the formation of Ni $(CO)_4$ on a Nb_2O_5 support leading to a more stable catalyst. $Ni(CO)_4$

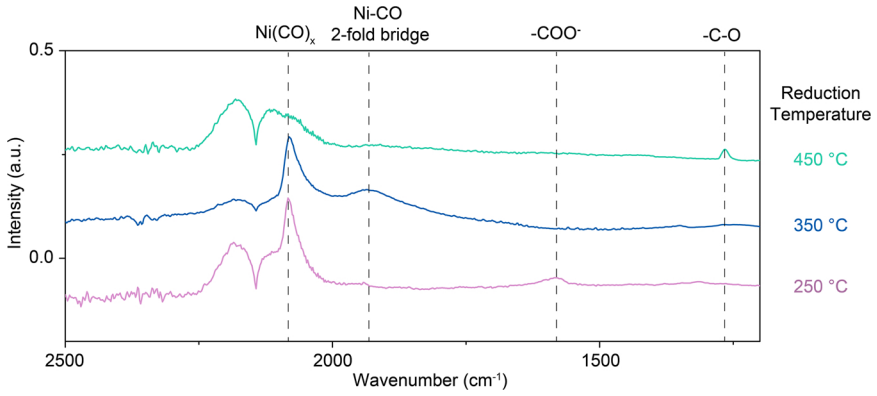

Fig. 5. FT-IR spectra of Ni/Nb_2O_5 after reduction at 250, 350 or 450 °C under CO atmosphere.

formation rate has been reported to depend on the nickel surface morphology with particularly low coordinated Ni atoms readily reacting to form carbonyls [46,47], thus NbO_x species might be responsible for blocking or modifying the electron density of these sites.

Fourier-Transform Infrared (FT-IR) spectroscopy was used to study the differences for the sample reduced at 250, 350 and 450 °C in their tendencies to form nickel carbonyl. *In-situ* reduction of the wafer was carried out at these three different temperatures. Thereafter FT-IR spectra were recorded at 230 °C under atmospheric pressure of $CO/N_2 = 2$ v/v flow (Fig. 5). Interestingly, a pronounced sharp band at 2080 cm^{-1} can be observed when the sample was reduced at 250 °C. This band is ascribed to subcarbonyl $Ni(CO)_x$ (x = 2, 3) species, precursors of $Ni(CO)_4$, in accordance with literature [47–49]. These species were also detected for the catalyst reduced at 350 °C and in both cases the band disappeared after flushing with N_2. In contrast, reduction at 450 °C did not give rise to this subcarbonyl $Ni(CO)_x$ band. These results show that there is a reduction temperature dependency in nickel carbonyl formation. Lower reduction temperatures thus most likely led to rapid deactivation during CO hydrogenation due to Ni particle growth via the formation and diffusion of $Ni(CO)_4$ originated from the detected $Ni(CO)_x$ species. High reduction temperature showed stable catalytic activity (Fig. 3), suggesting that the SMSI effect suppressed the formation of $Ni(CO)_x$ species and hence $Ni(CO)_4$, avoiding the diffusion of nickel over the support. Furthermore, the FT-IR spectra plotted in Fig. 5 show that the degree of CO activation in the adsorbed state is affected by the reduction temperature. That is, a reduction at 250 °C shows a large contribution of $Ni(CO)_x$ at 2090 cm^{-1} corresponding to the strongest carbon-oxygen bond based on the relatively high wavenumber of this band. A band at 1580 cm^{-1} is also observed which is attributed to carboxylate-type species, these may have originated from the oxidation of CO by the remaining NiO in this sample as shown by the TPR results. For a slightly higher reduction temperature (350 °C) besides the band at 2090 cm^{-1}, a broad peak at around 1960 cm^{-1} is observed, which is ascribed to C═O adsorbed in a 2-fold bridge position [50,51]. At the highest reduction temperature (i.e., 450 °C) a small peak at ~ 1266 cm^{-1} appears, which can be ascribed to the weakest CO bond [52], or lowest wavenumber observed in this set of experiments.

Two effects of the SMSI can explain the inhibition of nickel carbonyl formation. On one hand, NbO_x suboxides might physically block the more reactive low-coordinated Ni atoms on the surface of the nanoparticles, preventing the formation of subcarbonyl $Ni(CO)_x$ species. A similar effect has been shown in literature by addition of alkali metals or sulfur to nickel-based catalysts [53,54]. On the other hand, the suboxides partially covering the nickel nanoparticle's surface are capable of transferring electrons to the nickel [55–57]. In this case, Nb^{4+} or Nb^{3+} in the NbO_x suboxides might transfer electron density to the metallic nickel, resulting in electron-rich $Ni^{\delta-}$ atoms at the surface. Upon CO chemisorption at the nickel surface, $Ni^{\delta-}$ increases the back-donation to the CO $2\pi^*$ antibonding orbital weakening the C–O bond, as suggested by FT-IR, and thus avoiding the formation of $Ni(CO)_x$ species. Furthermore, an electron-rich metallic surface could hinder the re-adsorption of electron-rich molecules, explaining the increased olefin to paraffin ratios when the catalyst was reduced at high temperatures.

4. Conclusions

The effect of different reduction temperatures was studied for nickel nanoparticles supported on niobia. An increase of the reduction temperature led to H_2-chemisorption suppression, a typical phenomenon caused by reducible oxidic supports in which suboxides from the support cover partially the metal nanoparticles. The initial nickel-based catalytic activity was in line with the chemisorption results where high H_2-uptake corresponded to high initial CO conversion. However, low reduction temperatures turned into a fast deactivation due to nickel particle growth as shown by TEM, whereas a high reduction temperature led to stable catalytic performance and no significant particle growth. Interestingly, reduction of the niobia-supported catalyst at high temperature brought about an activation period during the first hours under reaction conditions followed by stable nickel-based activity. FT-IR measurements of CO adsorbed on Ni/Nb_2O_5 showed that nickel subcarbonyls readily formed after low but not after high reduction temperature. This could explain the particle growth involving the formation and diffusion of nickel tetracarbonyl, which formed from the detected nickel subcarbonyls. The inhibition of nickel tetracarbonyl formation after high temperature reduction is associated to the presence of suboxide species over the nickel surface, by either physically blocking exposed low-coordination nickel atoms, or by enhancing the electron density on the nickel surface and facilitating C–O bond rupture instead of nickel tetracarbonyl formation. The reduction treatment had a strong influence in the product distribution, where the highest selectivity towards C_{5+} was obtained after reduction at 350 °C, while a further increase of the reduction temperature shifted the product distribution towards lighter products. Finally, the promotional effect of reducible oxides, such as niobia, in CO hydrogenation was clearly shown since independently of the reduction temperature nickel supported on niobia showed higher nickel-based activity, TOF and C_{5+} selectivity compared to nickel supported on α-alumina, a non-reducible support. We have shown that niobia used as support material offers the possibility to make stable nickel-based catalysts for CO hydrogenation with tunable product spectrum.

Acknowledgments

Companhia Brasileira de Metalurgia e Mineração (CBMM) is thanked for financial support of this research. Dr. Robson Monteiro and Mr. Rogério Ribas (CBMM) are acknowledged for useful discussions and supplying the niobia support. Mr. Wouter Lamme (Utrecht University,

UU), Mrs. Petra Keijzer (UU) and Mrs. Savannah Turner (UU) are acknowledged for performing TEM measurements. KPdJ acknowledges the European Research Council (ERC) for a EU FP7 ERC Advanced Grant no. 338,846.

Appendix A. Supplementary data

Supplementary data associated with this article can be found, in the online version, at https://doi.org/10.1016/j.cattod.2018.11.036.

References

[1] P. Munnik, P.E. De Jongh, K.P. De Jong, Chem. Rev. 115 (2015) 6687–6718, https://doi.org/10.1021/cr500486u.
[2] C.H. Bartholomew, Appl. Catal. A Gen. 212 (2001) 17–60, https://doi.org/10.1016/S0926-860X(00)00843-7.
[3] E.D. Goodman, J.A. Schwalbe, M. Cargnello, ACS Catal. 7 (2017) 7156–7173, https://doi.org/10.1021/acscatal.7b01975.
[4] G. Prieto, J. Zečević, H. Friedrich, K.P. De Jong, P.E. De Jongh, Nat. Mater. 12 (2013) 34–39, https://doi.org/10.1038/nmat3471.
[5] C.E. Pompe, M. Slagter, P.E. de Jongh, K.P. de Jong, J. Catal. 365 (2018) 1–9, https://doi.org/10.1016/j.jcat.2018.06.014.
[6] D.E. Resasco, G.L. Haller, J. Catal. 82 (1983) 279–288, https://doi.org/10.1016/0021-9517(83)90194-X.
[7] X.Y. Shi, W. Zhang, C. Zhang, W.T. Zheng, H. Chen, J.G. Qi, J. Microsc. 262 (2016) 203–215, https://doi.org/10.1111/jmi.12366.
[8] S.J. Tauster, S.C. Fung, R.L. Garten, J. Am. Chem. Soc. 100 (1978) 170–175, https://doi.org/10.1021/ja00469a029.
[9] S.J. Tauster, Acc. Chem. Res. 20 (1987) 389–394, https://doi.org/10.1021/ar00143a001.
[10] M.A. Newton, Chem. Soc. Rev. 37 (2008) 2644–2657, https://doi.org/10.1039/b707746g.
[11] S. Zhang, P.N. Plessow, J.J. Willis, S. Dai, M. Xu, G.W. Graham, M. Cargnello, F. Abild-Pedersen, X. Pan, Nano Lett. 16 (2016) 4528–4534, https://doi.org/10.1021/acs.nanolett.6b01769.
[12] Y. Lykhach, S.M. Kozlov, T. Skála, A. Tovt, V. Stetsovych, N. Tsud, F. Dvořák, V. Johánek, A. Neitzel, J. Mysliveček, S. Fabris, V. Matolín, K.M. Neyman, J. Libuda, Nat. Mater. 15 (2015) 284–289, https://doi.org/10.1038/nmat4500.
[13] M.A. Vannice, R.L. Garten, J. Catal. 56 (1979) 236–248, https://doi.org/10.1016/0021-9517(79)90110-6.
[14] J. van de Loosdrecht, A.M. van der Kraan, A.J. van Dillen, J.W. Geus, J. Catal. 170 (1997) 217–226, https://doi.org/10.1006/jcat.1997.1741.
[15] E.I. Ko, J.M. Hupp, N.J. Wagner, J. Catal. 86 (1984) 315–327, https://doi.org/10.1016/0021-9517(84)90377-4.
[16] E.I. Ko, J.M. Hupp, N.J. Wagner, J. Chem. Soc. Chem. Commun. (1983) 94–95.
[17] G.B. Raupp, J.A. Dumesic, J. Catal. 96 (1985) 597–612, https://doi.org/10.1016/0021-9517(85)90327-6.
[18] Y. Lin, Y. Zhu, X. Pan, X. Bao, Catal. Sci. Technol. 7 (2017) 2813–2818, https://doi.org/10.1039/c7cy00124j.
[19] S. Shan, V. Petkov, L. Yang, J. Luo, P. Joseph, D. Mayzel, B. Prasai, L. Wang, M. Engelhard, C.J. Zhong, J. Am. Chem. Soc. 136 (2014) 7140–7151, https://doi.org/10.1021/ja5026744.
[20] Y. Li, Q. Fu, M. Flytzani-Stephanopoulos, Appl. Catal. B Environ. 27 (2000) 179–191, https://doi.org/10.1016/S0926-3373(00)00147-8.
[21] C. Vogt, E. Groeneveld, G. Kamsma, M. Nachtegaal, L. Lu, C.J. Kiely, P.H. Berben, F. Meirer, B.M. Weckhuysen, Nat. Catal. 1 (2018) 127–134, https://doi.org/10.1038/s41929-017-0016-y.
[22] L. Foppa, T. Margossian, S.M. Kim, C. Müller, C. Copéret, K. Larmier, A. Comas-Vives, J. Am. Chem. Soc. 139 (2017) 17128–17139, https://doi.org/10.1021/jacs.7b08984.
[23] Z. Li, L. Mo, Y. Kathiraser, S. Kawi, ACS Catal. 4 (2014) 1526–1536, https://doi.org/10.1021/cs401027p.
[24] W.M. Shen, J.A. Dumesic, C.G. Hill, J. Catal. 68 (1981) 152–165, https://doi.org/10.1016/0021-9517(81)90048-8.
[25] C. Mirodatos, H. Praliaud, M. Primet, J. Catal. 107 (1987) 275–287, https://doi.org/10.1016/0021-9517(87)90294-6.
[26] M. Agnelli, M. Kolb, C. Mirodatos, J. Catal. 148 (1994) 9–21, https://doi.org/10.1006/jcat.1998.1978.
[27] P. Munnik, M.E.Z. Velthoen, P.E. De Jongh, K.P. De Jong, C.J. Gommes, Angew. Chem. Int. Ed. 53 (2014) 9493–9497, https://doi.org/10.1002/anie.201404103.
[28] A. Cao, R. Lu, Phys. Chem. Chem. Phys. 12 (2010) 13499–13510, https://doi.org/10.1039/c0cp00729c.
[29] T.W. Hansen, A.T. Delariva, S.R. Challa, A.K. Datye, Acc. Chem. Res. 46 (2013) 1720–1730, https://doi.org/10.1021/ar3002427.
[30] W.M. Goldberger, D.F. Othmer, Ind. Eng. Chem. Process Des. Dev. 2 (1963) 202–209, https://doi.org/10.1021/i260007a006.
[31] B.C. Enger, A. Holmen, Catal. Rev. 54 (2012) 437–488, https://doi.org/10.1080/01614940.2012.670088.
[32] M.E. Dry, Catal. Today 71 (2002) 227–241, https://doi.org/10.1016/S0920-5861(01)00453-9.
[33] M. Agnelli, C. Mirodatos, J. Catal. 192 (2000) 204–214, https://doi.org/10.1006/jcat.2000.2828.
[34] E.B. Pereira, G.A. Martin, Appl. Catal. A : General. 103 (1993) 291–309.
[35] E. Zacharaki, P. Beato, R.R. Tiruvalam, K.J. Andersson, H. Fjellvåg, A.O. Sjåstad, Langmuir 33 (2017) 9836–9843, https://doi.org/10.1021/acs.langmuir.7b02197.
[36] H. Schäfer, R. Gruehn, F. Schulte, Angew. Chem. Int. Ed. Engl. 5 (1966) 40–52, https://doi.org/10.1002/anie.196600401.
[37] S.K.E. Forghany, J.S. Anderson, J. Chem. Soc., Dalt. Trans. (1981) 255–261, https://doi.org/10.1039/DT9810000255.
[38] D.J. Lensveld, J.G. Mesu, A.J. van Dillen, K.P. de Jong, Microporous Mesoporous Mater. 44–45 (2001) 401–407, https://doi.org/10.1016/S1387-1811(01)00214-1.
[39] B. Mile, D. Stirling, M.A. Zammitt, A. Lovell, M. Webb, J. Mol. Catal. 62 (1990) 179–198, https://doi.org/10.1016/0304-5102(90)85212-Z.
[40] S.K.E. Forghany, J.S. Anderson, J. Chem. Soc., Dalt. Trans. (1981) 255–261.
[41] C. Hernández Mejía, T.W. van Deelen, K.P. de Jong, Nat. Commun. 9 (2018) 4459, https://doi.org/10.1038/s41467-018-06903-w.
[42] C. Deleitenburg, A. Trovarelli, J. Catal. 156 (1995) 171–174, https://doi.org/10.1006/jcat.1995.1244.
[43] T. Komaya, A.T. Bell, J. Catal. 146 (1994), https://doi.org/10.1016/0021-9517(94)90027-2.
[44] E. Iglesia, S.C. Reyes, R.J. Madon, J. Catal. 129 (1991) 238–256, https://doi.org/10.1016/0021-9517(91)90027-2.
[45] C.H. Bartholomew, R.B. Pannell, J.L. Butler, J. Catal. 65 (1980) 335–347, https://doi.org/10.1016/0021-9517(80)90311-5.
[46] P. De Groot, M. Coulon, K. Dransfeld, Surf. Sci. 94 (1980) 204–220, https://doi.org/10.1016/0039-6028(80)90164-8.
[47] M. Agnelli, H.M. Swaan, C. Marquez-Alvarez, G.A. Martin, C. Mirodatos, J. Catal. 175 (1998) 117–128, https://doi.org/10.1006/jcat.1998.1978.
[48] D.G. Blackmond, E.I. Ko, J. Catal. 96 (1985) 210–221, https://doi.org/10.1016/0021-9517(85)90374-4.
[49] M. Mihaylov, K. Hadjiivanov, H. Knözinger, Catal. Lett. 76 (2001) 59–63, https://doi.org/10.1023/A:1016786023456.
[50] M. Courtois, S.J. Teichner, J. Catal. 135 (1962) 121–135.
[51] M. Trenary, K.J. Uram, J.T. Yates, Surf. Sci. 157 (1985) 512–538.
[52] G. Socrates, Infrared and Raman Characteristic Group Frequencies: Tables and Charts, third edition, John Wiley and Sons, Ltd, Chichester, 2001.
[53] M.L. Ang, U. Oemar, E.T. Saw, L. Mo, Y. Kathiraser, B.H. Chia, S. Kawi, ACS Catal. 4 (2014) 3237–3248, https://doi.org/10.1021/cs500915p.
[54] H.S. Bengaard, J.K. Nørskov, J. Sehested, B.S. Clausen, L.P. Nielsen, A.M. Molenbroek, J.R. Rostrup-Nielsen, J. Catal. 209 (2002) 365–384, https://doi.org/10.1006/jcat.2002.3579.
[55] C.C. Kao, S.C. Tsai, M.K. Bahl, Y.W. Chung, W.J. Lo, Surf. Sci. 95 (1980) 1–14, https://doi.org/10.1016/0039-6028(80)90126-0.
[56] W. Wang, X. Li, Y. Zhang, R. Zhang, H. Ge, J. Bi, M. Tang, Catal. Sci. Technol. 7 (2017) 4413–4421, https://doi.org/10.1039/C7CY01119A.
[57] M. Xu, S. He, H. Chen, G. Cui, L. Zheng, B. Wang, M. Wei, ACS Catal. 7 (2017) 7600–7609, https://doi.org/10.1021/acscatal.7b01951.